

Spontaneous decay of periodic magnetostatic equilibria

William E. East, Jonathan Zrake, Yajie Yuan, and Roger D. Blandford
*Kavli Institute for Particle Astrophysics and Cosmology, Stanford University,
SLAC National Accelerator Laboratory, Menlo Park, California 94025, USA*

We study a prototypical class of magnetostatic equilibria where the magnetic field satisfies $\nabla \times \mathbf{B} = \alpha \mathbf{B}$, where α is spatially uniform, on a periodic domain. Using numerical solutions of the force-free electrodynamic and relativistic ideal magnetohydrodynamic evolution equations, we show that generic examples of such equilibria are unstable to ideal modes which are marked by exponential growth in the linear phase. We characterize the unstable mode, showing how it can be understood in terms of merging magnetic and current structures and explicitly demonstrate its instability using the energy principle. Following the nonlinear evolution of these solutions, we find that they exhibit dissipation of magnetic energy and eventually settle into a configuration with the largest allowable wavelength. Such examples of magnetic energy being liberated on dynamical time-scales may have implications for astrophysical sources.

Introduction.—Magnetic stability is a fundamental question in a range of fields from laboratory plasma physics, where it influences the viability of fusion devices [1]; to space physics, where it controls the structure of magnetic fields within stars and planets; to high-energy astrophysics, where it governs the geometry of black hole [2, 3] and neutron star magnetospheres [4].

The explosive release of magnetic energy, as exemplified by coronal mass ejections [5], and more dramatically by magnetar flares [6–8], is most likely triggered by the spontaneous decay of a magnetic equilibrium. It is also conjectured that a mechanism of this type underlies powerful gamma-ray flares originating from the Crab nebula (as well as relativistic jets and gamma ray bursts)[9, 10]. The synchrotron emission observed during these flaring events requires the acceleration of electrons above 10^{15} eV energies with extremely high efficiency [11, 12], which in turn necessitates rapid, volumetric conversion of magnetic energy into high energy particles and radiation.

In this work, we focus on a prototypical class of space-periodic equilibria that satisfy the Beltrami property, $\nabla \times \mathbf{B} = \alpha \mathbf{B}$ with uniform α . Although there is a rich literature studying force-free magnetic equilibria, and the Beltrami solution in particular [13–16], fundamental questions about its stability, or lack thereof, are still unanswered. In [16] it was concluded that such solutions are linearly stable against incompressible deformations of the embedding medium (see also [17]). Here we use numerical simulations to show that generic periodic Beltrami magnetic fields are linearly unstable. The only exceptions we find are ones lacking magnetic curvature, and those in the fundamental mode or *ground state*, which have the lowest magnetic energy allowed by periodicity and the conservation of magnetic helicity $H_M = \int \mathbf{A} \cdot \mathbf{B} dV$ (where \mathbf{A} is the magnetic vector potential). We also explore the nonlinear evolution, finding strong evidence that transitions from excited states to the ground state occur on dynamical time scales. This behavior illustrates the rapid liberation of magnetic energy accompanying spontaneous loss of magnetic equilibrium.

It also reflects the general tendency for magnetic fields to assemble themselves over the largest available scale, a process known as inverse cascading [18–21].

In what follows, we outline our numerical methods, present results showing the linear-regime instability of a range of magnetostatic equilibria using force-free electrodynamic (FFE) simulations, and then illustrate the properties of the dominant unstable mode in an example case, explicitly confirming its growth rate using the energy principle. We compare these results to those found at finite magnetization, discussing the nonlinear evolution of the instability, and then conclude. We use units with $c = 1$ throughout.

Methodology.—The equilibrium magnetic fields we study are exemplified by the three-parameter “ABC” field [22] given by

$$\mathbf{B}^E = (B_3 \cos \alpha z - B_2 \sin \alpha y, \\ B_1 \cos \alpha x - B_3 \sin \alpha z, \\ B_2 \cos \alpha y - B_1 \sin \alpha x). \quad (1)$$

We use some particular examples of this equilibrium solution for illustrative purposes, but also consider the more general class of Beltrami fields [23]

$$\mathbf{B} = \alpha \Psi + \nabla \times \Psi \quad (2)$$

where the potential field Ψ is any solenoidal vector field satisfying the vector Helmholtz equation $\nabla^2 \Psi + \alpha^2 \Psi = 0$, so that Ψ comprises only the Fourier harmonics whose wave-vector \mathbf{k} has magnitude α . These more general configurations are constructed by choosing random vector amplitude for the admissible harmonics. Our computational domain is the periodic cube of length $L = 2\pi$ (though we restore L in some places for clarity).

We assume a perfectly conducting medium, and consider cases having both finite and infinite magnetization. The latter case corresponds to a magnetically dominated plasma where the inertia of its charge carriers may be neglected. This limit is treated by FFE [24, 25]. We numerically solve these equations using fourth-order finite

difference stencils and Runge-Kutta time stepping. We use the symmetric-hyperbolic formulation of the equations described in [26], combined with hyperbolic divergence cleaning to exponentially damp violations of the $\nabla \cdot \mathbf{B} = 0$ constraint. The $\mathbf{E} \cdot \mathbf{B} = 0$ constraint is explicitly enforced by redefining $\mathbf{E} \rightarrow \mathbf{E} - \mathbf{B}(\mathbf{E} \cdot \mathbf{B})/B^2$ at every coarse time step.

For finite magnetization cases, we solve the ideal relativistic magnetohydrodynamic (RMHD) equations. Our scheme is based on a second-order, finite-volume scheme that explicitly conserves mass, energy, momentum, and magnetic flux. We enforce $\nabla \cdot \mathbf{B} = 0$ via the constrained transport technique. Full details of the code are described in [27].

Instability in the Linear Regime.—For this class of magnetic equilibria, we find generic solutions with $\alpha^2 > 1$ to be unstable to linear ideal perturbations that are characterized by exponential growth of the electric field. Fig. 1 illustrates this for a case with $\alpha^2 = 11$. (Here we present results from FFE simulations, and in a later section we compare these to RMHD.) The magnitude of the growing solution is proportional to the initial perturbation¹, consistent with a linear instability. The growth rate of, e.g., the electric field energy is converging to $\gamma \approx 4.0\alpha/L$ with increased resolution, evidence that the instability is not due to numerical/non-ideal effects.

Equilibrium solutions with lower values of α^2 exhibit similar exponentially growing solutions, as shown in Fig. 2. This holds up until the fundamental mode for the domain, $\alpha^2 = 1$, which is known to be stable [16, 17]. The growth rate of the instability is also roughly proportional to α , though there is dependence on the particular realization used.

The Dominant Unstable Mode.—In order to illustrate the nature of the instability, we focus on a simple type of $\alpha = 2$ equilibrium solution given by Eq. 1. We illustrate this solution for three different choices of coefficients in Fig. 3. As discussed in [22] for the mathematically equivalent Euler flow, these solutions have a rich structure. The $(B_1, B_2, B_3) = (1, 1, 0)$ case consists of “vortices:” regions of helical field (and current) lines circling a central axis. The $(B_1, B_2, B_3) = (1, 1/2, 0)$ case has vortices as well as “shear layers:” wavy field lines that begin and end on opposite sides of the domain. In addition to these two cases with z -translational symmetry, we also show a more generic case where all three coefficients are nonzero (and that like the second case, has no places where $\mathbf{B}^E = 0$).

In Fig. 3 we also show the corresponding velocity field $\mathbf{v} = \mathbf{E} \times \mathbf{B}^E/|\mathbf{B}^E|^2$ (which will be proportional to the

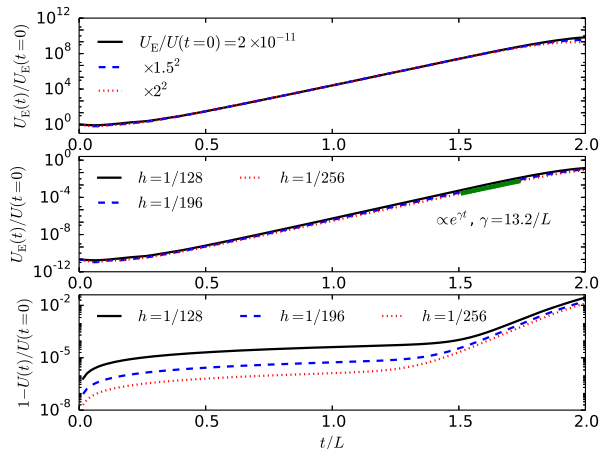


FIG. 1. Results from simulations with $\alpha^2 = 11$. Top: The growth of the electric field energy U_E , normalized by its initial value, for three different values of the initial perturbation. Middle: The exponential growth in U_E for three different resolutions, along with an exponential fit. The difference between the best fit exponent for the high resolution, and the Richardson extrapolated value using all three resolutions, is $\approx 0.1\%$, the extrapolation being consistent with between first and second-order convergence. The bottom panel illustrates the conservation of total energy U for three different resolutions. Early on, when the truncation of error of the equilibrium solution dominates, the convergence in this quantity is fifth-order, though eventually the convergence drops to roughly first-order, presumably because (as discussed below) the unstable solution has non-smooth features. The conservation of magnetic helicity is similar.

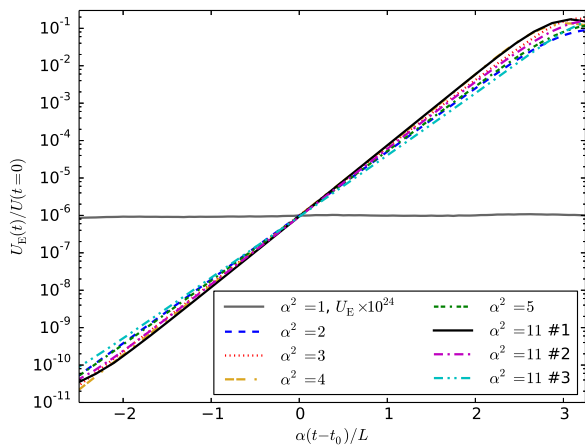


FIG. 2. The growth in electric field energy for various values of α^2 and three different realizations for $\alpha^2 = 11$. Time has been shifted so that all the curves have an abscissa of 0 at the ordinate value of 10^{-6} , and the time axis has been scaled by α which gives the different examples roughly the same slope. The $\alpha^2 = 1$ simulation does not exhibit exponential growth, and has been scaled up by an overall factor.

¹ Here the initial perturbation we use is an electric field with $E^x = E_0 \cos(2\pi y/L)$ and where the other components are given by cyclic permutations of $\{x, y, z\}$. From this we subtract out any component parallel to \mathbf{B} .

displacement for an eigenmode) characterizing the dominant instability arising in each case. This is calculated from a numerical snapshot after the instability has grown by roughly 10 orders of magnitude — seeded in this case just by truncation error — but is still in the linear regime ($|\mathbf{E}| \sim 10^{-4}|\mathbf{B}^E|$). The velocity field acts to bring together vortices circulating in the same direction in order to, as discussed below, move towards a larger wavelength, lower magnetic energy configuration. We can also see that the velocity field appears to have non-smooth features, reminiscent of spontaneous current sheets [28], that occur at the separatrices dividing the vortices and shear layers. The choice of where the vortices move towards or away from each other is what breaks the π/L -periodicity symmetry of the equilibrium solution. In fact, for the no-shear-layer case the velocity field in neighboring regions appears to have reflection symmetry about the separatrix line that divides them. Though the generic case lacks z -translational symmetry, it appears qualitatively similar to the second case.

From the $(B_1, B_2, B_3) = (1, 1, 0)$ to the $(1, 1/2, 0)$ case, the growth rate of the instability decreases by a factor of ≈ 1.9 with the addition of the shear layers in the equilibrium solution. In fact, the growth rate decreases monotonically with B_2 , and as $B_2 \rightarrow 0$ and the vortices shrink to zero volume, the growth rate of the instability also goes to zero (hence single mode solutions can be stable even at short wavelengths).

Focusing on the generic case, we note that this velocity is compressible with $\int |\nabla \cdot \mathbf{v}| dV \approx 0.15 \int |\nabla \times \mathbf{v}| dV$. We can also confirm the instability of this equilibrium to linear ideal perturbations by using the energy principle [29]. This implies that an equilibrium solution \mathbf{B}^E satisfying the Beltrami property is unstable to a displacement ξ if

$$\omega^2 := \frac{\int [|\delta\mathbf{B}|^2 - \alpha(\xi \times \mathbf{B}^E) \cdot \delta\mathbf{B}] dV}{\int |\mathbf{B}^E|^2 |\xi|^2 dV} < 0, \quad (3)$$

where $\delta\mathbf{B} := \nabla \times (\xi \times \mathbf{B}^E)$, and that the instability should grow at least as fast as $|\omega|$. Computing this quantity using finite differences, with the numerical velocity field, gives a value of $|\omega|L \approx 2.4$, near the growth rate of 2.6 measured for the electric field in the simulation. Furthermore, we can show that non-smooth features are not essential to a unstable perturbation by taking the numerical velocity field and filtering power at large wavenumbers to construct, e.g., an ideal perturbation that has no power at scales $|\mathbf{k}| > 29$ and gives a value of $|\omega|L \approx 2.3$ when Eq. (3) is calculated algebraically in k -space. Similar results are obtained for other unstable equilibria.

Finite magnetization cases and nonlinear evolution.— The same qualitative behavior is observed when the plasma magnetization is finite. Fig. 4 shows the evolution of the kinetic and magnetic energy U_B for different volume-averaged magnetization parameters $\sigma := \langle B^2/4\pi\rho h \rangle$ (where ρh is the fluid enthalpy density), including the limiting case of FFE, $\sigma = \infty$. The lower inset

of Fig. 4 shows that the growth rate of the unstable mode increases monotonically with increasing σ and is roughly proportional to the Alfvén speed $v_A = \sqrt{\sigma/(1+\sigma)}$.

In both finite and infinite magnetization cases, exponential growth of the unstable displacement persists until its velocity $|\mathbf{v}|$ approaches the Alfvén speed v_A (near the speed of light for large σ). At such time, higher-order evolutionary terms dominate and the motion becomes chaotic.

Following the turbulent state, the system settles into a lower energy equilibrium. Somewhat surprisingly, we *do not* observe the system to evolve directly into the lowest energy ($\alpha = 1$) state for all cases. For example, the $\alpha^2 = 11$ state in Fig. 4 first transitions into a configuration with $\approx 97\%$ of its spectral energy in modes with $\mathbf{k}^2 = 3$, where it remains for about ten Alfvén crossing times, before making a second transition into the ground state, where 99% of its energy is in $\mathbf{k}^2 = 1$ modes. The lifetime of the intermediate state may be related to the fact that $\approx 88\%$ of the energy is in a single $\mathbf{k}^2 = 3$ mode.

The non-linear evolution is characterized by coalescence of magnetic vortices or current channels, and can thus be related to the coalescence instability of magnetic islands [30]. This process is clearly illustrated in the $(B_1, B_2, B_3) = (1, 1, 0)$, $\alpha = 2$ configuration which has four current channels oriented in the $+z$ direction, and another four in the $-z$ direction (red and blue respectively in the top-left of Fig. 3). It is easy to see that all of the current channels of like sign can be made to lie within a single magnetic surface just by “snipping” the magnetic X-points in alternating directions. Doing so makes the topology similar to the corresponding $\alpha = 1$ configuration. Once all four of the, e.g., positive current channels lie within the same magnetic surface, non-ideal effects can bring about their mutual coalescence until only two vortex cores (or O-points) remain.

Such non-ideal effects are ultimately responsible for the dissipation of electromagnetic energy. Since we are evolving ideal systems whose formal solutions are energy-conserving, dissipation is effected in a somewhat arbitrary manner. The hyperbolicity of the FFE equations requires $|\mathbf{E}| < |\mathbf{B}|$, a constraint that nevertheless can be violated by formal FFE evolution, as happens in the nonlinear phase here. Numerically, we handle such regions with an ad-hoc prescription where we simply reduce the electric-field magnitude to equal that of the magnetic field, leading to a reduction of energy. Our RMHD evolution scheme explicitly conserves total energy, but permits conversion of magnetic or kinetic energy into internal energy, especially at shocks or places where the magnetic field is nearly discontinuous.

Although the energy dissipation is somewhat arbitrary, we still find consistency between the results of very different approaches. In particular, as shown in Fig. 4, we find the energy levels associated with the intermediate and final magnetic equilibria to be consistent with conserva-

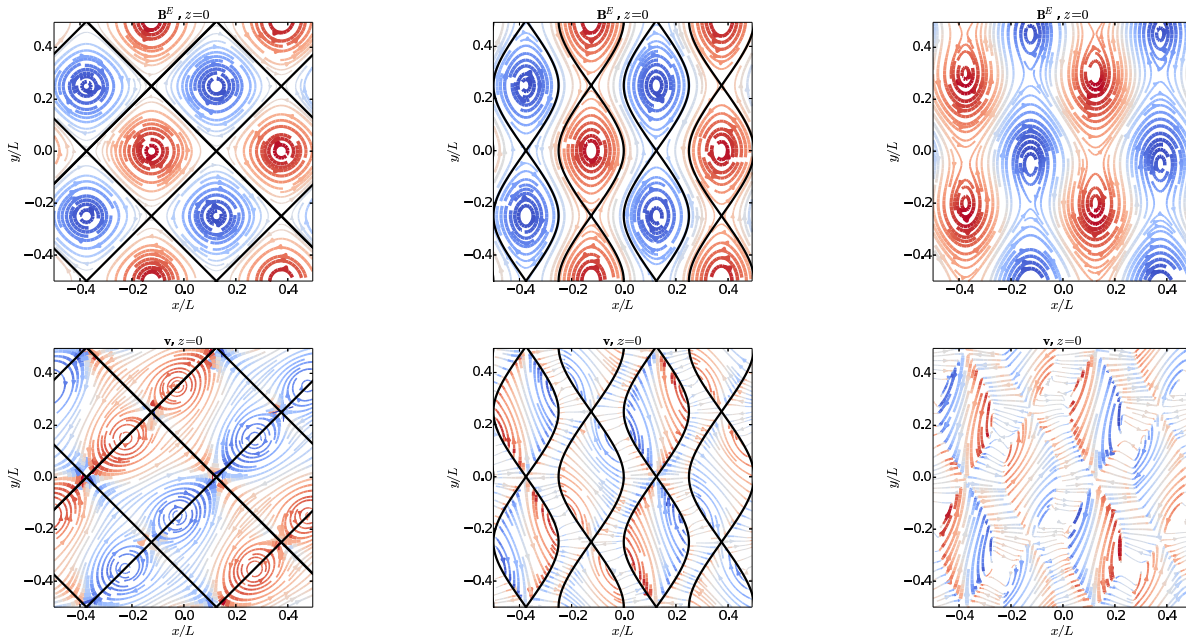


FIG. 3. Streamlines of a magnetic field equilibrium solution \mathbf{B}^E given by Eq. 1 with $\alpha = 2$ and various coefficients (top), and the corresponding velocity field $\mathbf{v} = \mathbf{E} \times \mathbf{B}^E / |\mathbf{B}^E|^2$ of the unstable mode arising from the simulations (bottom) in the $z = 0$ plane. The equilibrium solutions, from left to right, correspond to $(B_1, B_2, B_3) = (1, 1, 0)$, $(1, 1/2, 0)$, and $\approx (-0.814, 0.533, 0.232)$, respectively. The color indicates the perpendicular vector component with red and blue representing, respectively, out of the page and into the page. The thickness of the streamline is proportional to the vector magnitude. The black lines indicate the location of the separatrices in the equilibrium solutions.

tion of magnetic helicity. Since the Beltrami fields have $\mathbf{B} = \alpha \mathbf{A}$, their helicity is $2U_B/\alpha$, and the ratio of magnetic energy in the α_i and α_f equilibria is simply α_f/α_i . Accordingly, we do not expect the dissipation mechanism to have much influence on the energy in the final state, as long as helicity is preserved. For the simulations shown in Fig. 4, H_M is constant to $\sim 0.1\%$.

Conclusions.—We studied periodic Beltrami magnetic fields in the finite and infinite magnetization cases and found that generic cases exhibited instability, followed by turbulence, and eventually relaxed to the longest wavelength configuration. The instability quickly gives rise to regions where the electric field energy density is comparable to the magnetic field. In astrophysical sources where such configurations may be relevant, like the Crab pulsar wind, these would be likely sites of particle acceleration and photon emission, a possibility we will explore in future work.

Further exploration of the nonlinear regime will require physical modeling of the dissipation process, for example with resistive MHD or kinetic simulations incorporating radiative losses, which will reveal details of the plasma heating and, potentially, the energization of nonthermal particles. We also plan to study a broader class of magnetic equilibria, perhaps in spherical or cylindrical geometries.

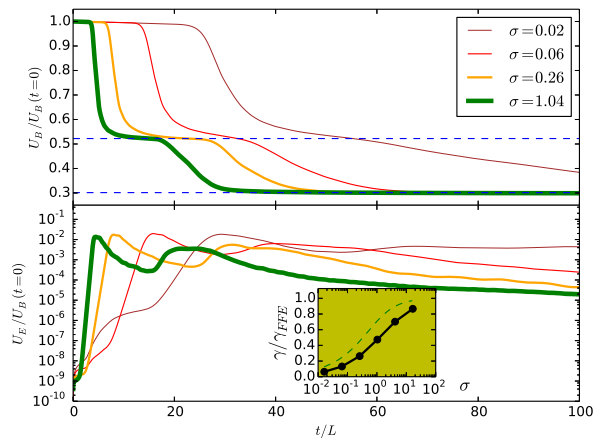


FIG. 4. A comparison of the decay of an $\alpha^2 = 11$ equilibrium in FFE and RMHD simulations with different values of magnetization parameter σ . Shown is the magnetic energy (top) and kinetic energy — or electric field energy in the case of FFE — (bottom). The top panel also shows, in horizontal dashed lines, the magnetic energy of $\alpha^2 = 3$ and $\alpha^2 = 1$ states with the same helicity. The bottom inset shows the linear growth rate γ measured for runs having different magnetization parameters, along with the Alfvén speed (dashed line) for comparison.

We thank Antony Jameson for useful conversations. YY and RB thank Keith Moffat for helpful advice and encouragement. This work was supported in part by the U.S. Department of Energy contract to SLAC no. DE-AC02-76SF00515, NSF grant AST 12-12195, as well as the Simons Foundation, the Humboldt Foundation, and the Miller Foundation (RB). YY gratefully acknowledges support from the KIPAC Gregory and Mary Chabolla fellowship and the Gabilan Fellowship awarded by Stanford University. Simulations were run on the Bullet Cluster at SLAC, the Sherlock Cluster at Stanford University, and using resources provided by the NASA High-End Computing (HEC) Program through the NASA Advanced Supercomputing (NAS) Division at Ames Research Center.

-
- [1] J. Freidberg, *Reviews of Modern Physics* **54**, 801 (1982).
 [2] R. D. Blandford and R. L. Znajek, *Monthly Notices of the Royal Astronomical Society* **179**, 433 (1977).
 [3] F. Zhang, S. T. McWilliams, and H. P. Pfeiffer, *ArXiv e-prints* (2015), 1501.05394.
 [4] P. Goldreich and W. H. Julian, *Astrophys. J.* **157**, 869 (1969).
 [5] K. Shibata and T. Magara, *Living Reviews in Solar Physics* **8** (2011).
 [6] C. Thompson and R. C. Duncan, *Monthly Notices of the Royal Astronomical Society* **275**, 255 (1995).
 [7] M. Lyutikov, *Monthly Notices of the Royal Astronomical Society* **367**, 1594 (2006).
 [8] C. Yu, *The Astrophysical Journal* **757**, 67 (2012).
 [9] R. Blandford, P. Simeon, and Y. Yuan, p. 14 (2014), 1409.2589.
 [10] R. Blandford, Y. Yuan, and J. Zrake, *American Astronomical Society* (2015).
 [11] A. A. Abdo *et al.*, *Science* (New York, N.Y.) **331**, 739 (2011).
 [12] M. Tavani *et al.*, *Science* (New York, N.Y.) **331**, 736 (2011), 1101.2311.
 [13] L. Woltjer, *The Astrophysical Journal* **128**, 384 (1958).
 [14] M. M. Molodensky, *Solar Physics* **39**, 393 (1974).
 [15] J. B. Taylor, *Physical Review Letters* **33**, 1139 (1974).
 [16] H. K. Moffatt, *Journal of Fluid Mechanics* **166**, 359 (1986).
 [17] M. Er-Riani, A. Naji, and M. El Jarroudi, *International Journal of Non-Linear Mechanics* **67**, 231 (2014).
 [18] U. Frisch, A. Pouquet, J. Leorat, and A. Mazure, *Journal of Fluid Mechanics* **68**, 769 (1975).
 [19] A. Alexakis, P. D. Mininni, and A. Pouquet, *The Astrophysical Journal* **640**, 335 (2006).
 [20] J. Zrake, *The Astrophysical Journal* **794**, L26 (2014).
 [21] A. Brandenburg, T. Kahniashvili, and A. G. Tevzadze, *Physical Review Letters* **114**, 075001 (2015).
 [22] T. Dombre, U. Frisch, M. Henon, J. M. Greene, and A. M. Soward, *Journal of Fluid Mechanics* **167**, 353 (1986).
 [23] S. Chandrasekhar and P. C. Kendall, *The Astrophysical Journal* **126**, 457 (1957).
 [24] T. Uchida, *Phys. Rev.* **E56**, 2181 (1997).
 [25] C. Thompson and O. Blaes, *Physical Review D (Particles)* **57**, 3219 (1998).
 [26] H. P. Pfeiffer and A. I. MacFadyen, p. 11 (2013), 1307.7782.
 [27] J. Zrake and A. I. MacFadyen, *The Astrophysical Journal* **744**, 32 (2011).
 [28] E. N. Parker, *Spontaneous current sheets in magnetic fields : with applications to stellar x-rays. International Series in Astronomy and Astrophysics, Vol. 1.* New York : Oxford University Press, 1994. **1** (1994).
 [29] I. B. Bernstein, E. A. Frieman, M. D. Kruskal, and R. M. Kulsrud, *Proceedings of the Royal Society of London A: Mathematical, Physical and Engineering Sciences* **244**, 17 (1958).
 [30] J. M. Finn and P. K. Kaw, *Physics of Fluids* **20**, 72 (1977).